Simulation of Fast-Rise Transients in a Large-Power Transformer Winding

Fuhua Li, *Member, IEEE*, Yilu Liu, *Fellow, IEEE*, Alfonso G. Tarditi, *Sr. Member, IEEE*, Zhi Li, *Member, IEEE*

***Abstract*——A High-altitude Electromagnetic Pulse (HEMP) may pose a significant threat to the electrical power grid. In this context, the present study considers the potential impact of the HEMP early-time component (E1) on the winding of a typical transmission power line transformer. A time-domain, fully electromagnetic, 3D, finite-element model was used to simulate the propagation of an E1-induced voltage surge into the transformer winding. The analysis is focused on the first few turns of the winding, the ones that are impacted by the largest electric field resulting from the applied pulse. The model follows the transient dynamics, while the pulse is traveling along the conductor, and the electric field is established across the insulation gaps through capacitive coupling. The simulations also considered the effect of an electrically floating, "shield" winding conductor. This is used as a countermeasure to improve the voltage uniformity across the winding during fast-rise transients. In this case, the propagation of the E1-induced pulse is compared with that from a slower rising, lightning standard waveform. The simulation results show that the presence of the shield conductor can effectively reduce the peak electric field between winding turns, in the presence of either E1 or lightning waveforms.**

***Index Terms*— High-altitude Electromagnetic Pulse (HEMP), Electromagnetic Transient, Power Line Surge, Transformer Winding.**

I. Introduction

The High-altitude Electromagnetic Pulse (HEMP) [1], due to its high peak electric field amplitude and fast-rise waveform, poses concerns for its possible damages to critical infrastructures, and in particular to the electric power grid.

Transformers are essential, and not easily replaceable, components of the transmission infrastructure, and they may be vulnerable to HEMP impact effects. This work considers the scenario where the early-time, fast-rise HEMP component (E1), after coupling to a power line [2], reaches the transformer winding. Compared to lightning surges, a typical E1 transient [3] is characterized by a much shorter rise time, reaching its peak amplitude within only a few nanoseconds. The E1-induced surge may be still too fast to trigger an effective surge arrestor suppression, and may reach the transformer interior, possibly resulting in insulation failure [4], especially in an overvoltage condition occurring in the first few turns of the winding.

Earlier investigations were conducted on a single-phase transformer by injecting a HEMP waveform with 100kV peak voltage [5]. In that case, only the response of the whole transformer was analyzed, without details on the dynamics of the EM transient in the transformer interior. This paper presents the results of a fully electromagnetic (EM), time-dependent, finite element method (FEM) model applied to the simulation of the fast-rise, E1-type transient propagation in a transformer winding. The model accounts for the impact of the winding conductors on the EM transient propagation, and computes the electric field distribution in the insulation between the winding turns.

The simulation results provide information on the ability of a specific winding design to withstand a given voltage surge waveform, much more accurately than an estimate based on the transformer's basic insulation level (BIL).

In order to reduce the nonuniformity of the voltage distribution across the winding during a transient, an electrically floating, inter-turn "shield" conductor is sometimes introduced in large power transformers. This study also evaluates the effectiveness of this inter-turn shield for an E1-type of pulse, and compares it with the case of a standard lightning waveform. By comparing the results with and without shield, it is found that the shield conductors are effective in reducing the maximum electric stress on the insulation also for the case of fast-rise E1 wave.

II. Transformer Winding Modeling

A. General Considerations

In this study, the model is based on a disk-type transformer winding, as illustrated in Fig. 1 where, for clarity, only the high-voltage (HV) winding discs are shown, while low-voltage (LV) winding, located between the HV winding and the iron core, is omitted. The HV winding directly connects to the overhead power transmission lines through a bushing and thus, in principle, can be impacted by any line surges residual that has not been suppressed by arrestors. This is the rationale for the specific analysis of E1-induced fast-transients here considered.

In general, for a given incident wave (such as in the HEMP IEC standard specifications [3]), the effect of the coupling with the power line conductor may lead to a waveform with a slower

Manuscript submitted on 06 Jan 2019. This work was supported by the U.S. Department of Energy, Office of Electricity Delivery and Energy Reliability under contract number DE-AC05-00OR22725, the National Science Foundation under NSF Award Number EEC-1041877, and the CURENT Industry Partnership Program.

F. Li and Y. Liu are with The Department of Electrical Engineering and Computer Science, The University of Tennessee, Knoxville, Tennessee 37996, USA (email: fli20@utk.edu; liu@utk.edu). A. G. Tarditi and Z. Li, as well as Y. Liu are with Oak Ridge National Laboratory, Oak Ridge, Tennessee 37831, USA (email: tarditiag@ornl.gov; liz2@ornl.gov).

rise time (*e.g.* [2]), since both the line propagation constant and angle of incidence may change the waveshape considerably.

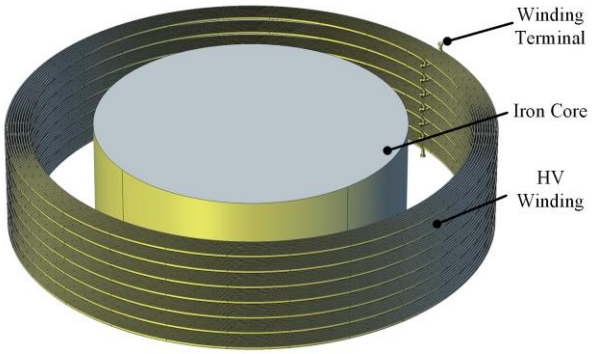

Fig. 1. A typical disk-type transformer winding segment.

Similarly, the transformer bushing may also provide a low-pass filtering effect that slows the rise time even further, but the actual impact on the waveform is strongly dependent on the bushing design geometry. For these reasons, this paper considers, as the worst-case scenario for pulse impact on the transformer winding, a conducted pulse injection with the same waveshape as the E1 incident wave. This provides the most stringent requirement on the design of the winding configuration in terms of reducing the vulnerability against HEMP threats.

Similar considerations could also be applied to LV windings, with the caveat that the coupling of the E1 incident wave is occurring typically on much shorter lengths, such as conductors inside a substations or generation plants, albeit at a lower operating voltage and BIL.

B. Preliminary Analysis: Equivalent Circuit

Following [6], an equivalent, approximate, circuit model for the transformer winding can be devised. Fig. 2-a shows an example of a simplified model for the first three turns of the winding. for each turn the ground capacitance C_g, series capacitance C_s, inductances $L_{1,2,3}$, (neglecting the conductor resistance) are defined as "effective", lumped element values resulting from the integration, over the length of the turn, of the corresponding distributed elements.

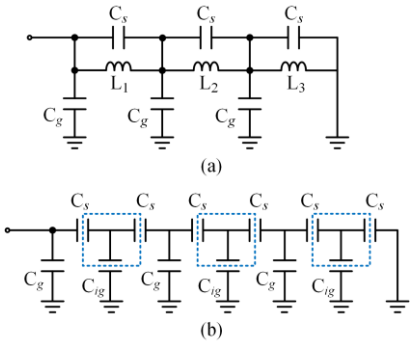

Fig. 2. (a) Equivalent circuit of a simplified transformer disc winding with distributed ground capacitance and series capacitance [6]. (b) Fast-transient equivalent circuit of a winding with inter-turn floating shield (Sect. II-C), inserted as indicated by dashed lines.

This model is approximated in that it neglects variations of the radius, among the different turns, but is deemed sufficiently accurate since the only three outermost turns are considered, thus leading to small relative variation for the radius.

For a fast-transient response, such as for an early-time E1 pulse, most of the energy in the transient is in the high-frequency components. As the frequency increases, the inductive reactance becomes larger, while the capacitive reactance gets smaller. In the 100's MHz range typical of the E1 spectrum, this leads to variations of orders of magnitude as compared to the values at the power frequency, Thus, in reference to the model in Fig. 2 applied to a high-frequency analysis, the winding inductance has little effect and can be neglected.

On the other hand, if a similar approach to the model of Fig. 2 was applied in a low-frequency range, the study of the transient should include the effect of the inductance.

As a result, for the propagation of a fast-rise E1-pulse, the winding equivalent circuit can include just the distributed ground and series capacitances, as in Fig. 2-b. The iron core is normally grounded, and it contributes to the winding ground capacitance. Since the distance between the winding and the core is much larger than the turn-to-turn distance, the ground capacitance introduced by the core is neglected in the model here considered.

As shown in [6], for a generic coordinate x along the winding length, an equation for the distribution of the (phasor) voltage $V_{wnd}(x)$ (defined with respect to the ground reference) can be derived as

$$\frac{d^2V_{wnd}}{dx^2} - \frac{1}{l^2}\frac{C_g}{C_s}V_{wnd} = 0 \tag{1}$$

that has the general solution

$$V_{wnd} = A_1 e^{px} + A_2 e^{-px} \tag{2}$$

where

$$p = \left(\sqrt{C_g/C_s}\right)\Big/ l \tag{3}$$

and A_1 and A_2 are two coefficients depending on the boundary conditions. The degree of approximation resulting from the application of this model to time intervals commensurate with the E1 propagation time scale, as considered in this paper, requires some careful examination. Nevertheless, some insight can be gained by observing that, as shown in (2) and (3), the ground-to-series capacitive ratio C_g/C_s is the key factor that determines the voltage distribution at the early time of the pulse propagation. A larger series capacitance C_s reduces p, and therefore the voltage V_{wnd}. C_s is mainly affected by the turn-to-turn and disk-to-disk capacitances, and by the dielectric constant of the insulator between the conductors.

C. Winding Design with Inter-Turn Shield

Different methods for increasing the series capacitance have been developed, including inter-turn winding shields, interleaved windings, and electrostatic shields. In [7], a disk-winding pair with wound-in-shield has been modeled to provide an estimate of the total series capacitance. This was performed by modeling both in the case of floating shield winding and the case with the shield connected to the input voltage. The changes in the series capacitance and its dependence on the number of

shield turns were then observed.

A similar inter-shield approach has also been used in [8] and [9], to improve the linearity of initial impulse voltage distribution across the different turns of the winding. Finally, a design with two electrostatic shields, connected to the line and the neutral ground, respectively, has been investigated in [10], showing that it provides an effective way to reduce the inter-winding dielectric stress resulting from surge voltages.

Another kind of shielded winding, based on a coaxial cable design, as shown in [14] for an application to broadband transformers, can be considered to minimize flux leakage. A related analysis could be performed also for power transformers, to improve the calculation accuracy of the propagation of the high-frequency pulse components.

Fig. 2-b shows the equivalent circuit of a disc winding applicable for fast-transients with the inter-turn floating shield conductor (enclosed by the dashed boxes). The presence of the shield leads to additional series capacitances (as shown later, in Fig. 4 and 6). For the purpose of providing a quick estimate of the effect of this configuration, it is here assumed that the shield conductor has the same insulation thickness and conductor height as the active winding turns, but smaller thickness.

The turn-to-shield capacitance is then same as C_s, the original turn-to-turn capacitance, since in both cases the overlapping area and insulator thickness are the same. However, now the overall turn-to-turn capacitance is the result of two equal capacitors C_s in series (thus resulting in a $C_s/2$ capacitance). It can also be observed that the floating shield has its own capacitance to ground (C_{ig} in Fig. 2-b), which is less than the ground capacitance C_g of each active turn, because the shield conductor thickness is smaller.

Thus, the overall effect of the floating shield is to reduce the ground-to-series capacitance ratio, and thus p, as in (3).

III. Winding Model

Simulations were performed to investigate the effectiveness of a floating inter-turn shield in reducing the uneven voltage distribution on a transformer winding during transient conditions.

In order to properly analyze the propagation of the transient, both the EM coupling in between turns as well as the propagation along the conductor winding need to be considered. Because the topology of the conductors and the high-frequency range are considered in this study, a transmission line modeling approach is not suitable for an accurate description of the pulse dynamics, and a full-wave, 3D electromagnetic model was then utilized.

The injection of three pulse waveforms was considered: a fast-rise E1 (as per IEC standard [3]), a modified, slower-rise E1, to account possible waveshape modifications (*e.g.* due to low-pass filtering effect, as discussed earlier), and a lightning standard pulse, for reference purpose.

The simulations provide a quantitative estimate of the maximum voltage reached across the insulation of the first few turns of the winding, thus allowing to determine if the basic insulation level (BIL) limit could be exceeded during transient conditions.

In the model, the first three turns of the HV winding are shown to be sufficient for analyzing the dynamics of the transient. This also allows to reduce significantly the complexity of the geometry and consequently the computational requirements, that however, due to the required spatial resolution, are still considerable. For reference, the simulations shown in this paper were obtained on a multi-core machine (20 Xeon cores and 128 GB RAM), and a run modeling dynamic response over 60 ns requires three to five days of actual computation time.

The HV winding model geometry was based on typical parameters for a large power transformer. More specifically, data for a 36 MVA 115/23 kV, BIL 350 kV were considered for reference, as listed in Table I.

TABLE I
Key Design Data

Winding inner diameter (mm)	1400
Wire height (mm)	10
Wire width (mm)	5
Turn-to-turn distance (mm)	3, 8.5
Shield height (mm)	10
Shield width (mm)	2.5
Turn-to shield distance (mm)	3
Winding terminal diameter (mm)	16
Iron core diameter (mm)	1000
Container diameter (mm)	1700

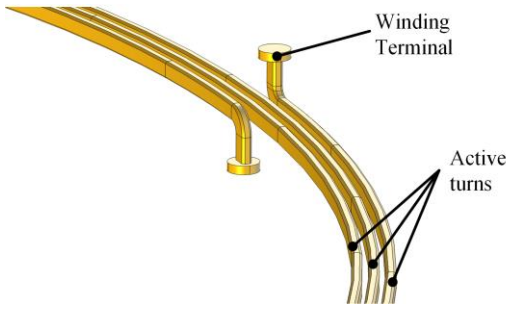

Fig. 3. The three-turn disc winding section model considered as reference.

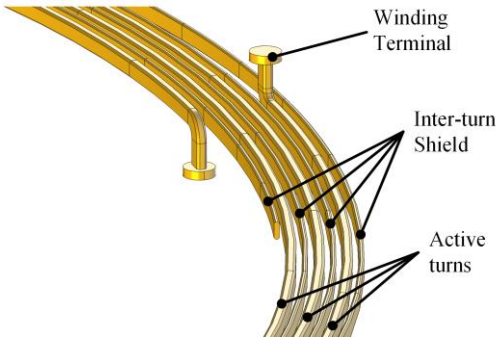

Fig. 4. Winding section with inter-turn shield, based on the one in Fig. 3

Fig. 3 shows the three-turn winding slice model with two terminals, represented by the short circular structures at the end of the vertical segments. In the simulation, the top terminal is connected to the excitation pulse source via a standard COMSOL coaxial-type port model [11]. This coaxial-type port provides an even voltage distribution all around the terminal, similar to a realistic bushing connection. The lower terminal is connected to a perfect conducting enclosure, simulating the grounded transformer case. This much shorter winding path to

the ground is here acceptable due to the short transients applied.

Fig. 4 displays the winding model with a floating inter-turn shield, here the shield thickness is considered as half of the active turn thickness. To enable a proper comparison, the turn-to-shield distance in the model of Fig. 4 is the same as the distance between active turns for the case (without shield) of Fig. 3.

As shown with the simple equivalent circuit model (1)-(3), a shield conductor thickness smaller than that of the active conductors reduces the ground capacitance. This, along with the reduced ground-to-series capacitive ratio C_g/C_s, is expected to lead to a reduced peak field, and thus an improved uniformity of transient voltage distribution.

IV. Simulation Results

The electromagnetic transient propagation in the winding was simulated with the 3D finite-element method (FEM), software package COMSOL Multiphysics (version 5.2a). In the simulation, the 3D winding slice models of Fig. 3 and 4 are inserted into a perfect electric conducting enclosure. The winding upper terminal is connected to a lumped-port for voltage injection [11] and the lower terminal is the ground connection to the enclosure.

The 3D FEM solution in COMSOL is computed on a tetrahedral mesh constructed on the interest regions. For a high-frequency analysis, the mesh element size is required to be smaller (e.g. at least about one fourth, or less) than the smallest wavelength being considered. For a 1 GHz upper frequency limit, the maximum element size should be then below 75 mm. While most of the E1 pulse energy is within a frequency range up to about 100 MHz, in order to insure more accurate results, in these simulations the mesh element size was here limited to 30 mm, *i.e.* one-tenth of the wavelength at 1 GHz.

Furthermore, since the wire thickness is only 5 mm, a much finer meshing was considered in the region immediately surrounding the winding conductors.

For the pulse injection the coaxial-type, lumped port COMSOL model is connected to a pulse voltage source of characteristic impedance Z_0. Here Z_0 is set as 400 Ohms, which is typical for an overhead transmission line [6], [12]. Since the pulse excitation scheme is kept the same for all the cases here considered, any difference in the simulations will be then only due to the winding characteristics.

The standard IEC-61000-2-9 double-exponential waveform for a HEMP-E1 component is considered [1], as:

$$E_1(t) = \begin{cases} 0 & , \ t \le 0 \\ E_{01} k_1 \left(e^{-bt} - e^{-at} \right), & t > 0 \end{cases} \tag{5}$$

$$k_1 = \left(\frac{a}{a-b} \right) \left(\frac{a}{b} \right)^{\left(\frac{b}{a-b} \right)} \tag{6}$$

where a and b determine the rise and decay time, respectively.

As it was discussed, in this study, a (possibly extreme) worst-case scenario, is first considered, corresponding to the situation where the waveshape on the power line induced by the E1 transient is not clamped by arrestors and is not affected by the transit through the bushing. Thus, in these conditions, an E1 waveform surge would be directly applied to the winding terminal. This is referred to as the "Fast-rise E1", 2.5/23 ns pulse, in Table II.

TABLE II
Pulse Waveforms

Wave type	a (s^{-1})	b (s^{-1})	Rise time / Width	Time to peak
Fast-rise E1	6.0×10^8	4.0×10^7	2.5 / 23.0 ns	4.8 ns
Slow-rise E1	6.0×10^7	4.0×10^6	25 / 229.8 ns	48.4 ns
Lightning	1.63×10^6	1.49×10^4	1.2 / 50 μs	2.9 μs

The IEC-61000-2-10 standard also recommends a 10/100 ns pulse for elevated lines and a 25/500 ns pulse for buried lines in a conducted environment [13]. Both these cases are considered with the "Slow-rise E1", 25/229.8 ns pulse, of Table II (that is about 10 times longer than the "Fast-rise E1"). This can be considered also as a realistic case where the protection of bushing and arrestor capacitance is affecting the waveshape.

Finally, for a more complete thorough analysis, a 1.2/50 μs lightning waveform, in Table II is also considered, as it is the typical reference transient that is accounted for in conventional winding designs.

A. Pulse Injection

The injected "Fast-rise" and "Slow-rise E1" waveforms, and the corresponding voltages on the winding terminal, are shown in Fig. 5, for both cases with and without shielding conductor. The terminal voltages differ from the ideal injected waveform due to the reflections from the winding.

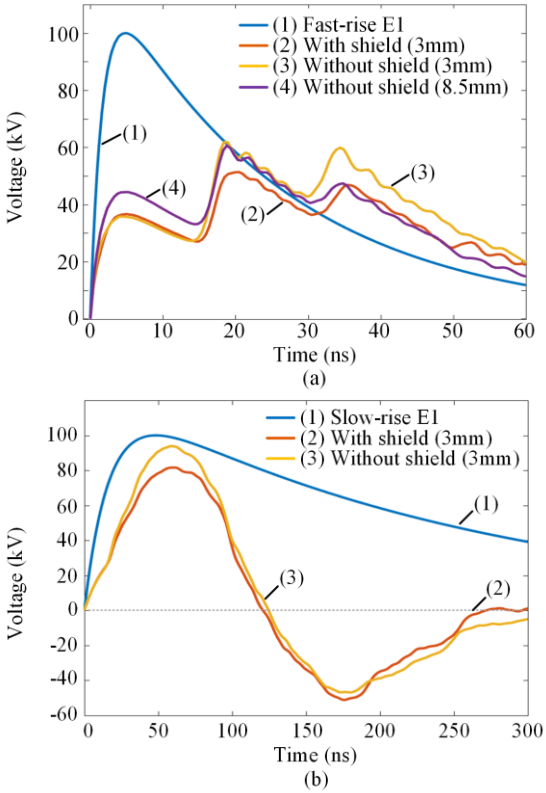

Fig. 5. Port voltage under (a) fast-rise and (b) slow-rise E1 HEMP wave. a-(1) Injected fast-rise E1 HEMP. a-(2) Winding with inter-turn shield. a-(3) Non-shielded winding with 3 mm turn-to-turn distance. a-(4) Non-shielded winding with 8.5 mm turn-to-turn distance.

In Fig. 5-a, for instance, it can be observed that the models with and without shield begin to differ after about 15 ns: that corresponds to the time required for the wave to travel along the entire circumference of the first turn, and then to reach the port location.

For a further comparison, the fast-rise E1 is also excited on a model without shield but with turn-to-turn spacing increased to 8.5 mm shown by curve (4) in Fig. 5-a. This is equivalent to replacing the floating shield with an insulator. It can be observed that during the initial 15 ns, curve (4) has the largest magnitude than the other two cases, because the series capacitance is reduced by the larger spacing. However, the ground capacitance changes only slightly, hence the winding impedance as seen from the port increases. Overall, the curve (4) shows that increasing the turn-to-turn distance does not reduce the amount of reflection back to the port or a transmission line.

Fig. 5-b displays the response to the slow-rise E1, that differs significantly from that resulting from the fast-rise E1 of Fig. 5-a, with a larger voltage response amplitude due to the larger energy provided by the input pulse. Curve (2) of Fig. 5-b also shows the effect of the shield winding, providing about 10% reduction in the simulated voltage.

B. Electric field

In the simulation, field probe locations have been defined to record the transient field components in between the winding turns, as well as on the conductor surface.

Fig. 6 shows the location of these "probes" for electric field, magnetic field, and current density (for a total of sixteen) on a cross-section plane perpendicular to the winding plane.

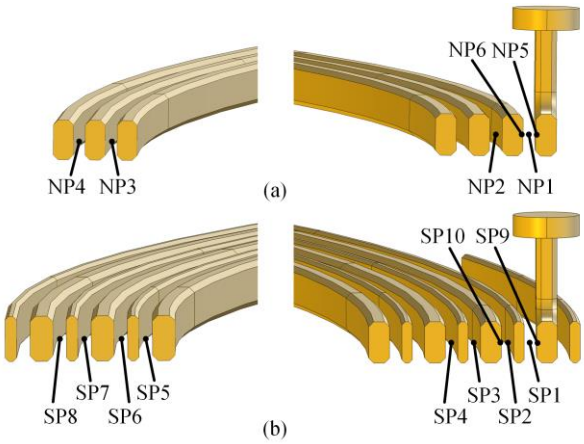

Fig. 6. Probe positioning on the winding with 3 mm spacing: NP indicates a probe in the non-shielded winding model, while SP refers the shielded case. (a) Original three-turn non-shielded winding. (b) Inter-turn shielded winding. NP1 − NP4 and SP1 − SP8: electric and magnetic field probes. NP5, NP6, SP9 and SP10: current density probes on the conductor surface points. The right cross-section is the side near the excitation port, and the left cross-section is the side far away from the port.

For example, as shown in Fig. 6-a, the non-shielded winding probe points NP1 and NP2 refer to the electric field in the middle of the gap. NP1 and NP2 correspond to the shielded winding probe points SP1 and SP2 of Fig. 6-b, respectively.

Fig. 7 and Fig. 8 compare the electric field magnitude (*i.e.* the norm or vector length of the field vector) in the insulation gap, respectively for the fast-rise and slow-rise E1 cases.

In Fig. 7-a, the field near the first turn (probes SP1, SP2 and NP1) show that the maximum electric field magnitude from SP1 (case with shield) is 7% lower than that from NP1 (case without shield). Also, the peak value from SP2 is 35% of that recorded by NP1.

The effect of the shield on the time waveform of the electric field magnitude recorded by probes near the second turn is shown in Fig. 7-b. The peak value with shield (recorded by SP3) is 70% of the corresponding value without shield (from NP2). Also, the peak from SP4 is 30% of that from NP2.

Fig. 7-c illustrates the results obtained from the probes placed on the opposite side of the winding, away from the excitation terminal. The shield leads to a reduction of the electric field between the second and the third turn by 20%.

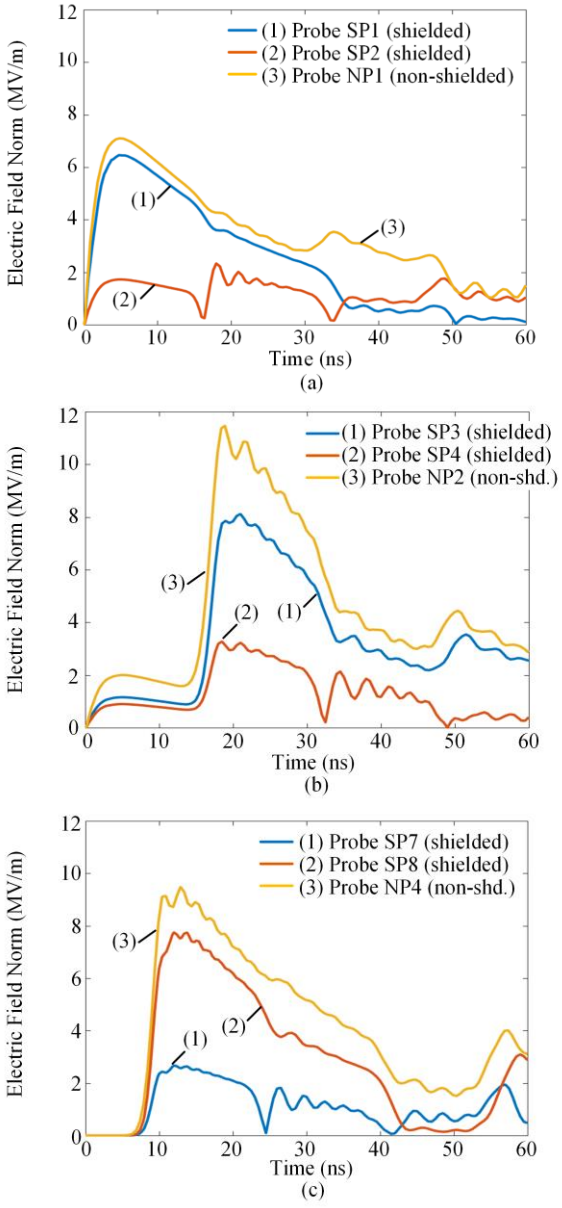

Fig. 7. Electric field magnitude excited by a fast-rise E1 pulse (only showing a few selected probes)

Fig. 8 summarizes the results with slow-rise E1. In all the three figures 8-a, b, c the zero value around 120 ns corresponds to the zero-crossing point for the applied port voltage in Fig. 5-b. The comparison of Fig. 8-a with the fast-rise results of Fig. 7-a, while accounting for the different scale in the horizontal axis, shows that the electric field increases more slowly, but reaches a higher amplitude. In Fig. 8-b the field shows a steep increase starting from 15 ns, similarly to the curves in Fig. 7-b. Likewise, in both Fig 7-c and Fig. 8-c the field increase occurs after a 7 ns delay (measured with respect to the applied voltage).

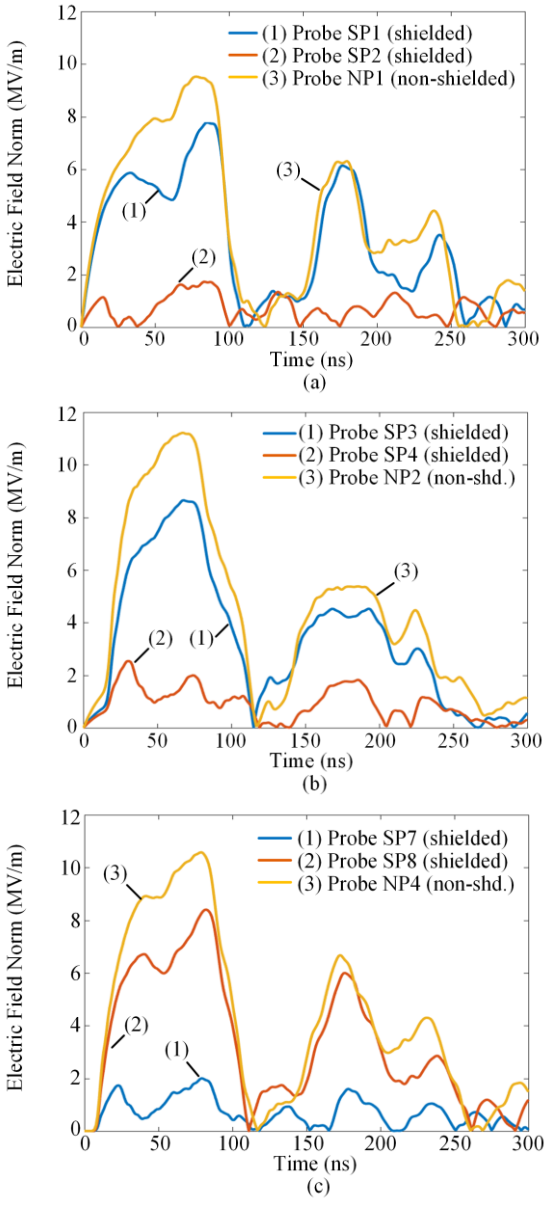

Fig. 8. Electric field magnitude excited by a slow-rise E1 pulse.

These results indicate that the two different pulses are affected by a similar delay, implying that the wave is traveling along the wire with the pulse delay being related only to the winding structure, as expected, and not to the excitation at the port. The specific value of this delay (several nanoseconds) is determined by the winding geometry, with the electric field resulting from both capacitive coupling and from the traveling wave along the conductor.

These results demonstrate that the floating shield can effectively reduce the electric field strength between winding turns under both fast-rise and slow-rise E1 excitation.

For instance, one can estimate the impact on possible insulator failures, from the simulation results shown in Fig. 7 and Fig. 8. In this case, with mineral oils insulation, with typical dielectric strength of 11.8 MV/m, an insulation failure or material contamination may occur. On the other hand, a winding built with calendered aramid paper (dielectric strength: 28.7 MV/m [15]) would be able to sustain the pulse transient.

The purpose of the simulation model here discussed is to show where the maximum field may be localized, thus in the model perfect insulators have been considered, as the physics of electric discharges is beyond the scope of this study.

A different visualization for this effect is shown through the electric field magnitude color map, as in Fig. 9 and Fig. 10, respectively for the non-shielded and shielded winding with 3 mm spacing. These are both the side view and top view plots, for the fast-rise E1 pulse case (as in Fig. 7).

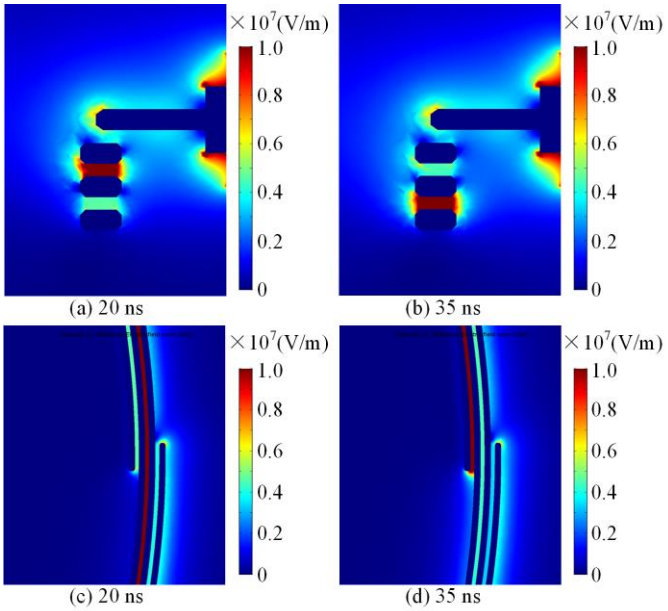

Fig. 9. Electric field norm excited by a fast-rise E1 pulse on the non-shielded winding with 3mm space. (a), (b) Cross section. (c), (d) Top view.

The different snapshots at the different times correspond to the peak points on the port voltage waveform shown in Fig. 5-a. For instance, in Fig. 9, at 20 ns, the wave peak (indicated by the red area) is located at the second conductor gap; then, at 35 ns, the pulse reaches the third conductor gap.

A similar pattern is noticeable for the shielded winding model in Fig. 10. Here the wave peak in the gap between turns is the result of capacitive coupling, while the conducted pulse propagates along the turns of the winding.

The electric field in Fig. 10 reaches a lesser intensity (lighter red color) as compared to Fig. 9, showing that the shield is indeed effective in reducing the turn-to-turn dielectric stress.

A more direct comparison is illustrated in Fig. 11, for the electric field magnitude on the winding surface of the two models of Fig. 9 and 10 at 20 ns, the time when the field reaches

its peak as shown in Fig. 7-b. The dark-red area on the conductor surface of non-shielded winding in Fig. 11-a corresponds to the lighter-red area on the shielded winding in Fig. 11-b, consistently with the conclusion that the presence of the floating shield reduces the electric field between winding turns.

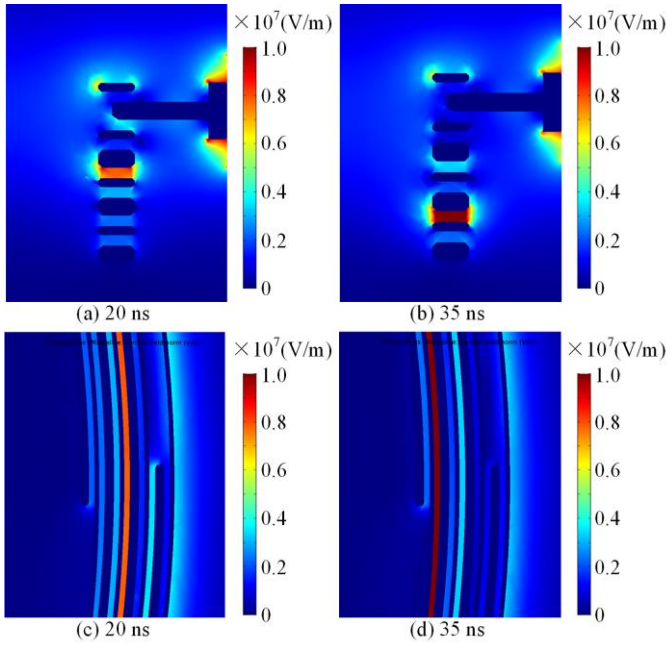

Fig. 10. Electric field norm excited by a fast-rise E1 pulse on the shielded winding with 3mm space. (a), (b) Cross section. (c), (d) Top view.

In summary, the three-turn model here considered, while very simplified as compared to an actual transformer, is effective for showing the dynamics of the traveling wave front along the winding, and of the related electric field rise in the gap between the adjacent conductors.

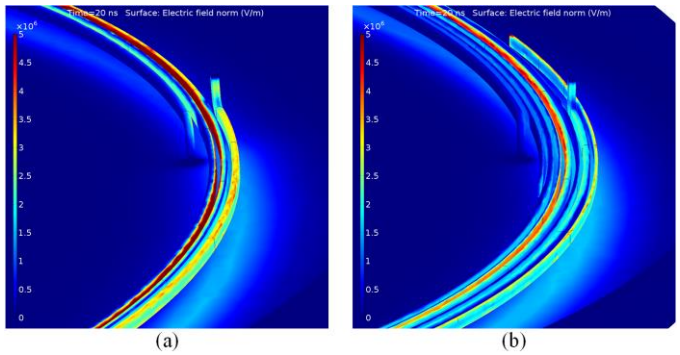

Fig. 11. Surface electric field magnitude at 20 ns excited by a fast-rise E1 pulse. (a) Non-shielded. (b) Shielded.

C. *Magnetic field*

The propagation of the wave excited by the pulse can be also observed in the magnetic field component, that is directly related to currents on the conductor surface. Fig. 12 displays the magnetic field magnitude recorded from probes on both the shielded and non-shielded winding.

Fig. 12-a shows the waveforms excited by a fast-rise E1, and the magnitude increase after 30 ns that is due to the wave reflection. Fig. 12-b illustrates the case for the slow-rise E1 pulse. Also, the pulse peak delays are consistent with the electric field shown in Fig. 7 and Fig. 8.

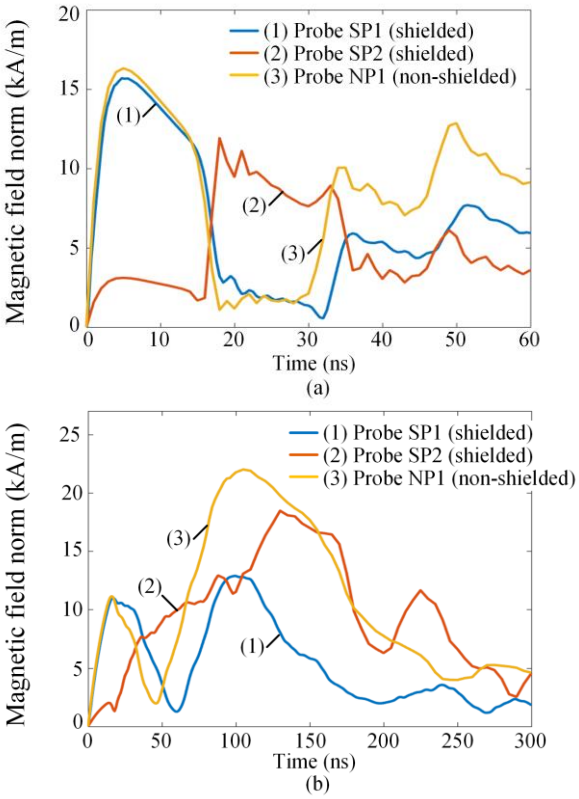

Fig. 12. Magnetic field magnitude recorded from the probes SP1, SP2 and NP1. (a) Excited by a fast-rise E1 pulse. (b) Excited by a slow-rise E1 pulse.

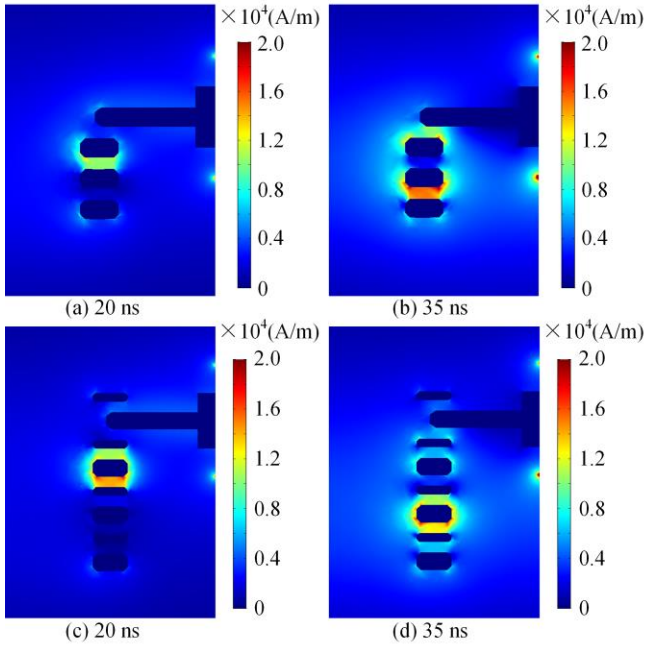

Fig. 13. Magnetic field norm distribution excited by a fast-rise E1 pulse on the winding with 3 mm space. (a), (b) non-shielded winding. (c), (d) shielded winding.

A color map of magnetic field magnitude for the fast-rise E1 case is shown in Fig. 13, both with and without floating shield.

The propagation pattern is consistent with that of the electric field component, as in Fig. 9 and 10.

D. Baseline Comparison

The previous results have shown the reduction of the electric stress due to presence of the inter-turn floating shield. For a further confirmation, two models without shield, but with a different insulation spacing are compared. This is intended to verify that the improved uniformity of the voltage distribution across the turns is indeed due to the presence of the shield, and not just to a larger insulation spacing that reduces the inter-turn capacitances. In this case, the simulations have been performed only conducted with a fast-rise E1 pulse, the most critical one.

The first case is the original model with a 3 mm turn-to-turn space, while in the second one, an 8.5 mm turn-to-turn spacing is considered, that is equivalent to the spacing between active turns in the shielded model.

Increasing the turn-to-turn spacing decreases the series capacitance and thus increases the ground-to-series capacitance ratio, as previously discussed in the model of eqs. (1)-(3). The results here presented show that, although increasing the turn-to-turn spacing reduces the electric field intensity between turns, the uniformity of the voltage distribution is not improved.

The instantaneous voltages between winding turns, were defined as in Fig. 14, and were calculated by straight-line integration of the electric field between turns. V_{N1}, V_{N2}, V_{N3} and V_{N4}, denote the turn-to-turn voltages in the model with the (narrow) 3 mm space. V_{W1}, V_{W2}, V_{W3} and V_{W4}, indicate the voltages for the 8.5 mm (wide) spacing case.

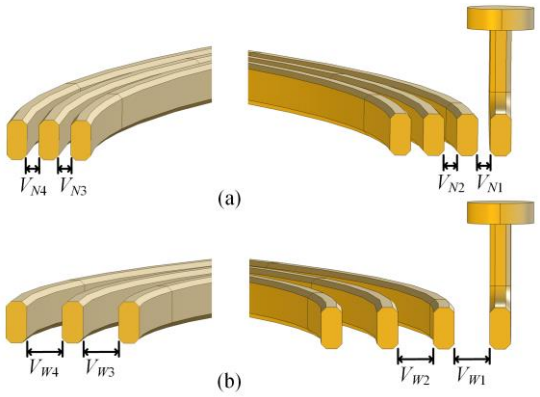

Fig. 14. Two winding models showing selected voltages between turns: (a) 3.5 mm spacing, and (b) 8.5 mm spacing.

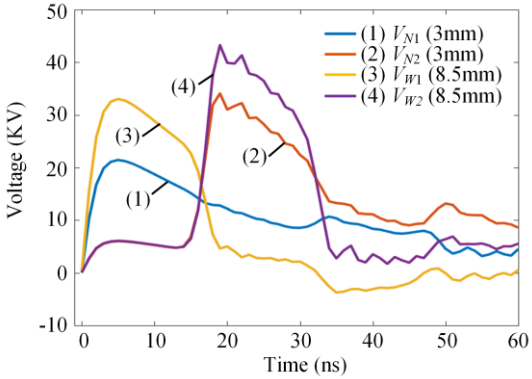

Fig. 15. Turn-to-turn voltage at the side near the excitation port.

In Fig. 15 these turn-to-turn voltages (resulting from the applied fast-rise E1) are plotted vs. time. The model with narrow (3 mm) gap shows a lower turn-to-turn voltage: V_{N1} is 65% of that of V_{W1}, and V_{N2} is 79% of V_{W2}. On the other hand, the peak voltages due to the wave propagation occurs almost at the same time, in the two cases.

Fig. 16 displays the turn-to-turn voltage on the side away from the excitation port. As in the previous comparison, the initial period with nearly zero voltage (about 7 ns), corresponds to the time required for the wave front to reach the probe location. In this case V_{N3} is 77% of V_{W3}, and V_{N4} is 70% of V_{W4}, consistently with the result in Fig. 15.

The curves of Fig. 15 and Fig. 16 show that the peak voltage between turns occurs sequentially on the probes V_{N1}, V_{N4}, V_{N2} and V_{N3}, as the pulse propagates to the inner section while traveling along the winding.

By comparing the results of the two models of Fig. 14-a and Fig. 14-b, it can be concluded that the larger the spacing, the larger the turn-to-turn voltage. This is unlike what was shown in the previous cases of sections IV-B and -C, thus confirming the conclusion that when the shield is introduced in the wider gap, the inter-turn voltage decreases.

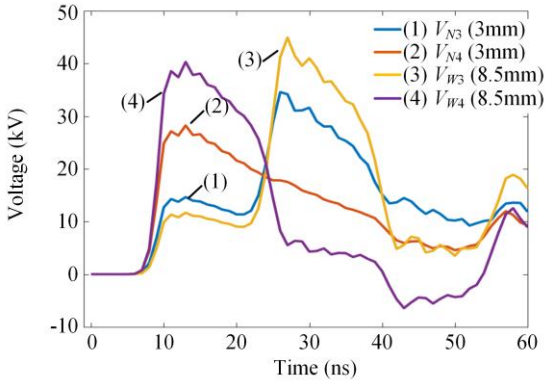

Fig. 16. Turn-to-turn voltage at the side away from the excitation port.

E. Lightning Pulse Waveform

The previous sections have discussed the cases excited by a fast-rise and a slow-rise HEMP E1 pulse. It can be found, from Fig. 7 and Fig. 8, that the electric field increases when the pulse width increases, *i.e.* when the waveform rising front is slower.

This section examines then the winding response when the pulse width is increased (the pulse rising gets slower), beyond the range of HEMP-E1 range, up to the typical lighting transients, and analyzes the effectiveness of the floating inter-turn shield. This case is considered for showing consistency with the previous simulations, while providing a validation for the typical transient regime that motivated in first place the introduction of the floating shield design for transformer windings.

For this purpose, a standard 1.2/50 μs lightning impulse waveform (as per IEEE Std 4-2013) is considered. The same reference voltage amplitude (100 kV) is applied, as in the previous simulations.

Fig. 17 shows the port voltage of the two models with 3 mm conductor spacing (as in Fig. 6), with the lightning pulse

waveform injection. As expected, the port voltage is much lower than that in the case of the E1 excitation in Fig. 5.

A closer examination shows the voltage amplitude of the winding with shield is 10% lower than that of the winding without shield. This indicates that the reflection of the lightning waveform is less than that in the fast-rise E1 case.

Furthermore, even the applied amplitude is same as that in the E1 case, the induced port voltage is much lower, showing a significantly increased loading of the transmission line feed.

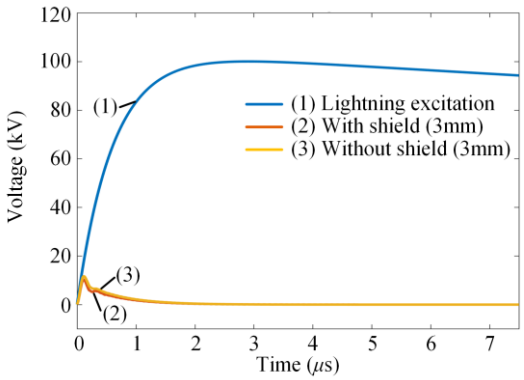

Fig. 17. Port voltage with and without shield, with 3 mm conductor spacing, from 1.2/50 μs lightning pulse voltage waveform injection.

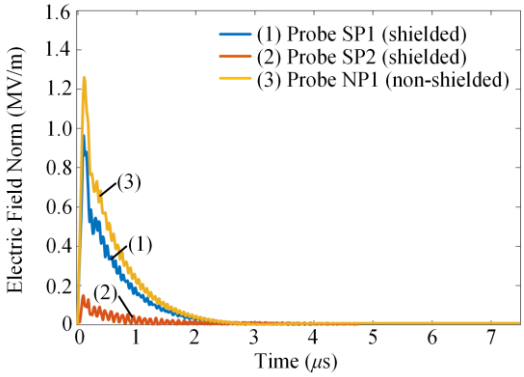

Fig. 18. Electric field magnitude near the 1st turn, with and without shield, for the lightning pulse waveform injection.

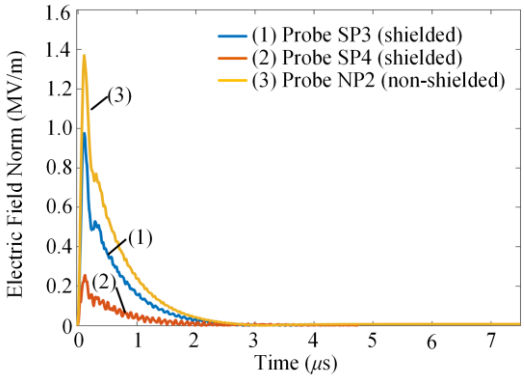

Fig.19. Electric field magnitude near the 2nd turn, with and without shield, for the lightning pulse waveform injection.

Fig. 18 shows the electric field from the probes placed half-way in the insulation between turns, as in Fig. 6. The comparison with Fig. 8 indicates that, for the cases with and without shield, the electric field induced by the lightning pulse wave is much less than the corresponding one from an E1 pulse. This analysis also shows that for the lightning pulse waveform, the presence of floating shield is more effective, as compared to the slow-rise E1 pulse, in reducing the non-uniformity of the voltage across the different gaps of the winding turns.

Fig. 19 illustrates the results near the second turn. As in Fig. 18, the electric field amplitude induced by the lighting impulse is lower than that induced by E1 pulse, and the winding with floating shield is under lower dielectric stress between conductors than in the case without shield, consistently with the previous result.

It is then apparent that, as expected, from the dielectric stress perspective, a fast-rise pulse (such as the E1 cases considered) has a more severe impact on the winding, than for a slower-rising pulse (such as a lightning transient), for the same given amplitude. These results also indicate that the inter-turn shield is effective in reducing the peak electric field strength between conductors in both situations, albeit less effectively for the faster risetime.

V. Conclusion

This paper discussed the response of a transformer winding to transient waveforms (considered within a range from faster to slower rise time), as may result from a HEMP environment coupled to an overhead transmission line, and then propagating into a transformer connected at the line termination. The fast-rise E1 waveform here considered represents the worst-case of HEMP coupling to transmission line, when there is no significant impact on the waveform from the line impedance and from the capacitances of bushings and arresters at the transformer terminals.

On the other hand, the slow-rise E1 represents a more realistic case where some low-pass filtering effect has impacted the waveform that reaches the winding.

The voltage transient leads to a voltage non-uniformity on the winding, and the insulation gaps between the first few winding turns are subject to a larger dielectric stress than the remaining ones.

For this analysis, a model consisting of the first three turns of a transformer winding is considered in order to examine in detail the field propagation during the transient response. The simulation results show the propagation of the electric and magnetic field components due to both capacitive coupling and the conducted wave traveling along conductor.

A comparison between the cases of E1 pulses and that of a 1.2/50 μs lightning transient shows that, for the same amplitude, the slower E1 pulse, due to its longer duration, induces a larger electric field in between the winding turns. However, the fast-rise E1 pulse results in the fastest electric field change, and thus larger non-uniformity. The electric field induced by the lighting pulse is much lower than that induced by an E1 pulse.

The effectiveness of a floating shield winding design in reducing the transient voltage non-uniformity between the turns, thus reducing the risk of insulation failures, was also examined. For this purpose, both winding models with and without shield, have been considered by applying voltage transients corresponding to a fast-rise E1, a slow-rise E1, and a

1.2/50 μs standard lightning pulse.

The simulation results show that the floating shield can effectively reduce the electric field intensity between winding turns both, for the lightning pulse and for the E1 case, albeit by a lesser amount for the latter (or in general when the risetime is reduced). This finding is also consistent with a simple network equivalent model based on the inter-electrode capacitances.

REFERENCES

[1] R. Hoad and W. A. Radasky, "Progress in High-Altitude Electromagnetic Pulse (HEMP) Standardization," *IEEE Trans. Electromagn. Compat.*, vol. 55, no. 3, pp. 532-538, Jun 2013.

[2] R. G. Olsen and A. G. Tarditi, "EMP Coupling to a Straight Conductor Above Ground: Transmission Line Formulation Based on Electromagnetic Reciprocity," *IEEE Trans. Electromagn. Compat.*, pp. 1-9, Jun 2018.

[3] D. V. Giri and W. D. Prather, "High-Altitude Electromagnetic Pulse (HEMP) Risetime Evolution of Technology and Standards Exclusively for E1 Environment," *IEEE Trans. Electromagn. Compat.*, vol. 55, no. 3, pp. 484-491, Jun 2013.

[4] M. Florkowski, J. Furgal and P. Pajak, "Analysis of fast transient voltage distributions in transformer windings under different insulation conditions," *IEEE Trans. Dielectr. Electr. Insul.*, vol. 19, no. 6, pp. 1991-1998, Dec 2012.

[5] F. M. Tesche and P. R. Barnes, "The HEMP response of an overhead power distribution line," in IEEE Transactions on Power Delivery, vol. 4, no. 3, pp. 1937-1944, July 1989.

[6] Allan Greenwood, Electrical transients in power systems. New York, NY, USA: Wiley, 1991, pp. 322–349, 551.

[7] R. M. Del Vecchio, B. Poulin and R. Ahuja, "Calculation and measurement of winding disk capacitances with wound-in-shields," *IEEE Trans. Power Del.*, vol. 13, no. 2, pp. 503-509, Apr 1998.

[8] M. Bagheri, B. T. Phung and M. S. Naderi, "Impulse voltage distribution and frequency response of intershield windings," *IEEE Elect. Insul. Mag.*, vol. 32, no. 5, pp. 32-40, Oct 2016.

[9] M. Bagheri, A. Hekmati, R. Heidarzadeh and M. Salay Naderi, "Impulse voltage distribution in intershield disk winding VS interleaved and continuous disk winding in power transformer," in *Proc. Int. Conf. Power and Energy*, Johor Bahru, 2008, pp. 387-392.

[10] B. Adamczyk, M. Florkowski and M. Swiatkowski, "Effect of shielding on surge overvoltages in multilayer type windings of power transformer," *IEEE Trans. Dielectr. Electr. Insul.*, vol. 23, no. 3, pp. 1627-1635, Jun 2016.

[11] COMSOL Multiphysics 5.2a RF Module User's Guide, COMSOL Inc., Burlington, MA, USA, 2016, pp.42-45.

[12] W. A. Radasky, "The application of IEC 61000-2-10 to establish E1 HEMP external conductor protection specifications," 2012 Asia-Pacific Symposium on Electromagnetic Compatibility, Singapore, 2012, pp. 345-348.

[13] M. W. Wik and W. A. Radasky, "Development of high-power electromagnetic (HPEM) standards," *IEEE Trans. Electromagn. Compat.*, vol. 46, no. 3, pp. 439-445, Aug 2004.

[14] C. E. Baum, "Winding topology for transformers," *IEEE Trans. Electromagn. Compat.*, vol. 30, no. 3, pp. 358-363, Aug. 1988

[15] John R. Rumble, "Dielectric strength of insulating materials." in *CRC Handbook of Chemistry and Physics*, 99th ed., Boca Raton, FL, USA: CRC Press, 2018, pp. 15-43 - 15-47.